PNAS PLUS

RhoA knockout fibroblasts lose tumor-inhibitory capacity in vitro and promote tumor growth in vivo

Twana Alkasalias[a,b], Andrey Alexeyenko[a,c], Katharina Hennig[d], Frida Danielsson[c], Robert Jan Lebbink[e], Matthew Fielden[f], S. Pauliina Turunen[a], Kaisa Lehti[a,g], Vladimir Kashuba[a,h], Harsha S. Madapura[a], Benedek Bozoky[a], Emma Lundberg[i], Martial Balland[d], Hayrettin Guvén[a], George Klein[a,1], Annica K. B. Gad[j,1,2], and Tatiana Pavlova[a,1,2]

[a]Department of Microbiology, Tumour, and Cell Biology, Karolinska Institutet, 17177 Stockholm, Sweden; [b]Department of Biology, College of Science, Salahaddin University, 44002, Irbil, Kurdistan-Iraq; [c]National Bioinformatics Infrastructure Sweden, Science for Life Laboratory, Karolinska Institute, 17177 Stockholm, Sweden; [d]Laboratoire Interdisciplinaire de Physique, Université Joseph Fourier (Grenoble 1), 38402 Saint Martin d'Hères Cedex 9, France; [e]Department of Medical Microbiology, University Medical Centre Utrecht, 3584 CX Utrecht, The Netherlands; [f]Department of Applied Physics, Nanostructure Physics, Kungliga Tekniska Högskolan Royal Institute of Technology, Albanova University Center, 106 91 Stockholm, Sweden; [g]Research Programmes Unit, Genome-Scale Biology, University of Helsinki, Finnish Cancer Institute, F1-00014 Helsinki, Finland; [h]Department of Molecular Oncogenetics, Institute of Molecular Biology and Genetics, National Academy of Sciences of Ukraine, 01004 Kiev, Ukraine; [i]Cell Profiling Facility, Science for Life Laboratory, Kungliga Tekniska Högskolan Royal Institute of Technology, 17177 Stockholm, Sweden; and [j]Science for Life Laboratory, Division of Translational Medicine and Chemical Biology, Department of Medical Biochemistry and Biophysics, Karolinska Institutet, 17177 Stockholm, Sweden

Contributed by George Klein, January 6, 2017 (sent for review August 17, 2016); reviewed by Hakan Axelson and Peter H. Krammer)

Fibroblasts are a main player in the tumor-inhibitory microenvironment. Upon tumor initiation and progression, fibroblasts can lose their tumor-inhibitory capacity and promote tumor growth. The molecular mechanisms that underlie this switch have not been defined completely. Previously, we identified four proteins overexpressed in cancer-associated fibroblasts and linked to Rho GTPase signaling. Here, we show that knocking out the Ras homolog family member A (*RhoA*) gene in normal fibroblasts decreased their tumor-inhibitory capacity, as judged by neighbor suppression in vitro and accompanied by promotion of tumor growth in vivo. This also induced PC3 cancer cell motility and increased colony size in 2D cultures. RhoA knockout in fibroblasts induced vimentin intermediate filament reorganization, accompanied by reduced contractile force and increased stiffness of cells. There was also loss of wide F-actin stress fibers and large focal adhesions. In addition, we observed a significant loss of α-smooth muscle actin, which indicates a difference between RhoA knockout fibroblasts and classic cancer-associated fibroblasts. In 3D collagen matrix, RhoA knockout reduced fibroblast branching and meshwork formation and resulted in more compactly clustered tumor-cell colonies in coculture with PC3 cells, which might boost tumor stem-like properties. Coculturing RhoA knockout fibroblasts and PC3 cells induced expression of proinflammatory genes in both. Inflammatory mediators may induce tumor cell stemness. Network enrichment analysis of transcriptomic changes, however, revealed that the Rho signaling pathway per se was significantly triggered only after coculturing with tumor cells. Taken together, our findings in vivo and in vitro indicate that Rho signaling governs the inhibitory effects by fibroblasts on tumor-cell growth.

Rho GTPases | RhoA | cancer-associated fibroblasts | tumor-inhibitory capacity | cytoskeleton

The tumor microenvironment consists of various cells and extracellular matrix (ECM) proteins, which together form the tumor stroma. This stroma differs from normal tissue in that it is highly enriched in ECM proteins, which form fibrous networks that provide scaffolds for tumor-cell proliferation and migration. Defective organization and composition of the ECM can thus influence tumor growth and metastasis (1–4). The architecture of the stroma mainly depends on the composition of the ECM and the mechanical and biochemical functions of fibroblasts (5).

Fibroblasts can inhibit growth of cancer cells (6, 7). The ECM and soluble factors that are secreted upon fibroblast–tumor cell contact drive the fibroblast inhibitory effects (8). However, this inhibitory activity of fibroblasts can be lost, and even reversed, to provide an opposing tumor stimulatory activity during tumor development (9). In parallel, fibroblasts activate proinflammatory gene expression (10). These activatory fibroblasts are often referred to as cancer- or carcinoma-associated fibroblasts (CAFs), and they have been suggested to promote tumor growth and metastasis through remodeling of the ECM network and cytokine and chemokine secretion (11).

Small Rho GTPases control the shape and mechanical and adhesive properties of fibroblasts (12). Most notably, RhoA (Ras homolog family member A) has been shown to induce assembly of focal adhesions and F-actin stress fibers, and to control the shape and adhesive and contractile properties of fibroblasts, as well as their capacity to organize the ECM (13, 14). CAFs often express myofibroblast markers, such as α-smooth muscle actin (α-SMA). We recently identified 12 markers that are highly

Significance

In order for cancer to develop, normal tumor-inhibitory fibroblasts need to change into tumor-promoting, cancer-associated fibroblasts. We created Ras homolog family member A (*RhoA*) gene knockout fibroblasts and found that even though these cells lacked common markers of classic cancer-associated fibroblasts, they had lost their normal tumor-inhibitory capacity and induced tumor-cell migration and proliferation in vitro and tumor growth in vivo. *RhoA* knock-out cells also showed an altered cytoskeleton, reduced contractile force, and induced stiffness of the fibroblasts. *RhoA* knockout also induced a loss of α-smooth muscle actin and an activated proinflammatory state, which was reflected by interference with a number of Rho signaling cascades. Our data indicate that RhoA is a key regulator of the switch from tumor-inhibitory to tumor-promoting fibroblasts.

Author contributions: T.A., G.K., A.K.B.G., and T.P. designed research; T.A., K.H., F.D., R.J.L., S.P.T., V.K., H.S.M., H.G., A.K.B.G., and T.P. performed research; T.A., A.A., R.J.L., M.F., S.P.T., K.L., M.B., and T.P. contributed new reagents/analytic tools; T.A., A.A., K.H., F.D., M.F., S.P.T., K.L., V.K., B.B., E.L., G.K., A.K.B.G., and T.P. analyzed data; and T.A., A.A., S.P.T., K.L., H.G., G.K., A.K.B.G., and T.P. wrote the paper.

Reviewers: H.A., Lund University; and P.H.K., German Cancer Research Center.

The authors declare no conflict of interest.

Freely available online through the PNAS open access option.

Data deposition: The data reported in this paper have been deposited in the Gene Expression Omnibus (GEO) database, www.ncbi.nlm.nih.gov/geo (accession no. GSE83913).

[1]To whom correspondence may be addressed. Email: georg.klein@ki.se, Annica.Gad@ki.se, or tatiana.pavlova@ki.se.

[2]A.K.B.G. and T.P. contributed equally to this work.

This article contains supporting information online at www.pnas.org/lookup/suppl/doi:10.1073/pnas.1621161114/-/DCSupplemental.

expressed in cancer-associated stroma and not in normal stroma (15). Four of these markers, DLG1, ROCK2, ARHGAP31, and ARHGAP26, are linked to Rho GTPase signaling. In that study, we also identified the known CAF marker ACTA2 (encodes α-SMA), which is regulated by the Rho GTPase signaling pathway (16–19). This link to the Rho pathway prompted us to hypothesize that RhoA signaling in fibroblasts mediates their capacity to control tumor growth.

Recent findings have indicated that an actomyosin-based contractile force in fibroblasts is required for CAFs to remodel the ECM (20). The stiffness of the extracellular environment can activate RhoA in fibroblasts, which leads to increased expression of (the CAF marker) α-SMA and differentiation into myofibroblasts (16, 17, 19). In line with this, Calvo et al. have suggested that CAFs can increase the stiffness of the ECM to stimulate the formation of CAFs, which results in a feed-forward, self-reinforcing loop, through which CAFs can promote tumorigenesis (20).

Taken together, these observations suggested that tumor growth and invasion is shaped by cross-talk between mechanical and biochemical signaling, which is modulated by RhoA signaling in fibroblasts. Therefore, targeting this pathway in fibroblasts might influence their tumor-inhibition capacity.

Results

RhoA Is Required for the Tumor-Inhibitory Capacity of Fibroblasts in Vitro and in Vivo. To determine whether RhoA affects the tumor-regulatory capacity of fibroblasts, we ablated RhoA in Bj human telomerase reverse transcriptase (BjhTERT) fibroblasts. Endogenous RhoA expression in control fibroblasts and significant loss of *RhoA* gene and protein expression in RhoA knockout (KO) BjhTERT fibroblasts was confirmed by quantitative RT-PCR (qRT-PCR) ($P < 10^{-6}$) (Fig. 1*A* and Fig. S1*A*) and Western blotting (Fig. 1*B*).

To determine the regulatory capacity of these fibroblasts on tumor cells, proliferation of PC3 prostate cancer cells was measured in vitro in monocultures and in cocultures with either control or RhoA-KO fibroblasts. Consistent with previous reports (6), coculture with control fibroblasts dramatically decreased PC3 cell growth (Fig. 1*C*), whereas RhoA-KO fibroblasts showed significantly decreased inhibition of PC3 cell growth, compared with control fibroblasts ($P < 10^{-10}$) (Fig. 1*C* and Figs. S1*B* and S2).

We then asked whether this RhoA deficiency of fibroblasts can also regulate tumor-cell growth in vivo in SCID or SCID-beige mice. Here, 2×10^4 PC3 cells were injected subcutaneously alone and in combination with 1×10^6 of either control or RhoA-KO fibroblasts. Across three repeated experiments, this relatively low number of PC3 cells alone did not induce any detectable tumorigenic response in the 9 wk following their injection. Coinjection of control fibroblasts with PC3 cells resulted in the formation of one small tumor in one of the five mice in two of the three experiments (Fig. 1*D* and Fig. S3). However, all of the mice injected with PC3 cells plus RhoA-KO fibroblasts developed tumors (Fig. 1*D* and Fig. S3) across the three experiments. After prolonged initiation over the initial 6 to 7 wk, these subcutaneous tumors then grew extremely rapidly, reaching volumes of up to 1 cm^3 within the following 2 wk (Fig. 1*D*). These experiments demonstrate that fibroblasts that lack RhoA do not inhibit tumor-cell growth both in vitro and in vivo.

In the following sections, we report on our investigation into how the RhoA KO in these BjhTERT fibroblasts altered cell morphology and dynamics, gene expression, and the impact of RhoA KO on the signaling network.

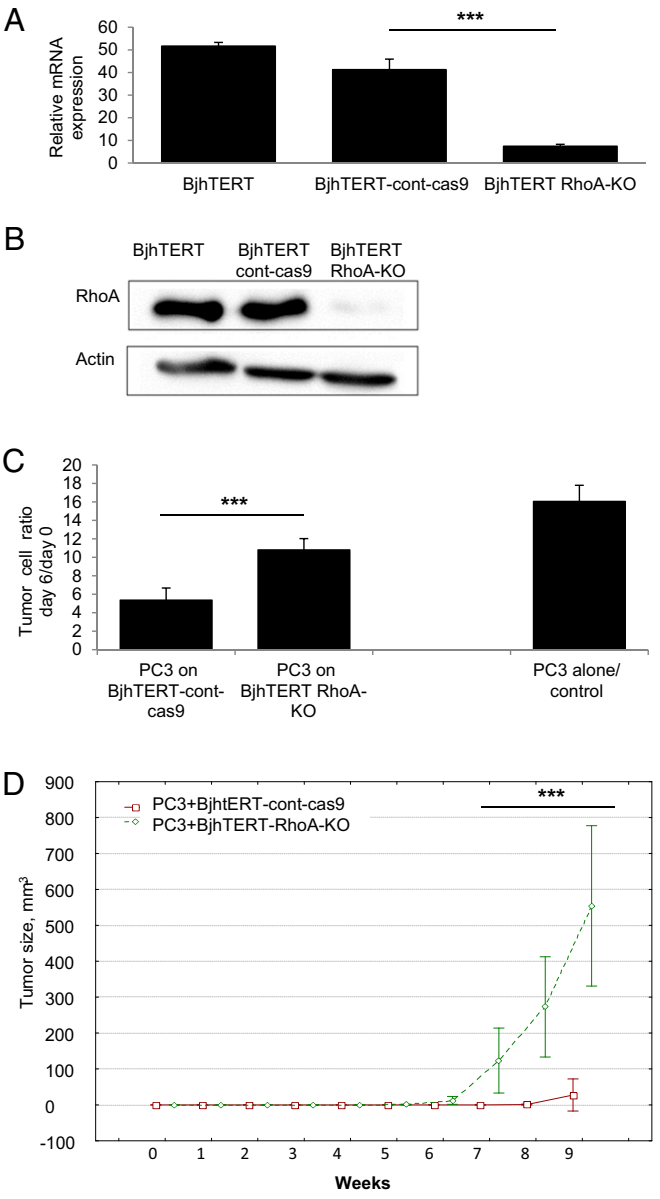

Fig. 1. Loss of RhoA in human fibroblasts reduces their tumor-inhibitory capacity in vitro and induces their tumor-stimulatory capacity in vivo. (*A*) qRT-PCR for RhoA expression in BjhTERT, BjhTERT–cont-cas9, and BjhTERT RhoA-KO fibroblasts. The *y* axis indicates the values of expression level of RhoA gene normalized to the *TBP* reference gene. The *x* axis shows the cDNA samples. Data are means with 0.95 confidence intervals. ***P = 0.00029 (one-way ANOVA with three levels). (*B*) Representative Western blots of BjhTERT, BjhTERT–cont-cas9 and BjhTERT RhoA-KO fibroblasts, for RhoA protein levels in total cell lysate (as indicated). Actin protein levels are shown as loading control. (*C*) Inhibitory capacity of BjhTERT–cont-cas9 and BjhTERT RhoA-KO fibroblasts as confluent monolayers (4-d-old) tested in coculture with PC3 mRFP prostate cancer cells. Data are proliferation ratios of PC3 mRFP cells after 6 d coculture with fibroblasts. ***$P < 10^{-10}$. (*D*) Tumor volumes in SCID mice injected with mixtures of PC3 mRFP cells with BjhTERT–cont-cas9 fibroblasts or BjhTERT RhoA-KO fibroblasts (as indicated). PC3 mRFP alone and with BjhTERT fibroblasts did not form tumors (not shown for clarity). Data are means of three independent experiments. ***$P < 10^{-10}$. See details and statistical analysis in Fig. S3.

RhoA-KO Fibroblasts Induce Tumor-Cell Motility and Proliferation. To study the mode of interaction of RhoA-KO fibroblasts with tumor cells, we examined the differences in the motility of PC3 mRFP cells (PC3 cells stably expressing monomeric red fluorescent protein) in coculture with control and RhoA-KO fibroblasts using total internal reflection fluorescence (TIRF) microscopy for live-cell time-lapse imaging. PC3 mRFP cell motility was recorded for 65 h, with these 65 (hourly) time points subdivided into five color-coded trajectories whereby each corresponded to 13 h of recording. Similar to their effect on PC3 cell proliferation in

vitro, the inhibitory effect of fibroblasts on cell motility of PC3 was significantly decreased upon knocking out the RhoA gene in fibroblasts ($P = 0.0037$) (Fig. 2 and Movies S1 and S2). Furthermore, in the RhoA-KO fibroblast cocultures, PC3 mRFP cells formed larger colonies than when cocultured with control fibroblasts, as measured by the distribution of the PC3 mRFP cells over a given area (Fig. S4 and Movies S3 and S4). Consistent with the contact-dependent neighbor suppression described by Alkasalias et al. (8), early contacts at the beginning of the cocultures between the fibroblasts and PC3 mRFP cells were essential to inhibit tumor-cell proliferation and motility. Remarkably, this inhibition was lost with the RhoA KO/deficiency of the RhoA-KO fibroblasts (Movies S5 and S6).

Altered Cytoskeleton and Adhesion Structures in RhoA-KO Fibroblasts Are Linked to Changes in Cellular Contractile Force and Stiffness. Control and RhoA-KO fibroblasts were examined under immunofluorescence microscopy, where the RhoA deficiency resulted in less regularly shaped cells compared with those of control fibroblasts (Fig. 3). Furthermore, RhoA-KO fibroblasts showed less formation of wide actin stress fibers and fewer distinct, dense, and large focal adhesions (Fig. 3*A*). RhoA-KO fibroblasts also showed significant reduction in α-SMA expression (Fig. S5). Furthermore, the structure of vimentin intermediate filaments in RhoA-KO cells appeared less organized, and in a more homogenous distribution of very thin and long filament extensions throughout the cell cytoplasm (Fig. 3*B*).

To determine whether this altered cytoskeleton structure of RhoA-KO fibroblasts was associated with changes in the mechanical properties of these cells, their contractile force and stiffness were measured using traction force and atomic force microscopy, respectively. Compared with control fibroblasts, RhoA-KO fibroblasts showed significantly reduced contractile forces ($P = 0.004$) (Fig. 4*A*). In contrast, the cell stiffness, here represented by the elastic modulus determined via indentation of the cells, was more homogenous and more evenly distributed for RhoA-KO fibroblasts than control fibroblasts (Fig. 4*B*). When the cell areas were analyzed in detail, RhoA-KO fibroblasts appeared significantly stiffer than control fibroblasts ($P = 0.0196$) (Fig. 4 *C* and *D*). RhoA-KO fibroblasts also showed lower numbers of very soft locations, compared with control fibroblasts (Fig. 4 *B* and *C*).

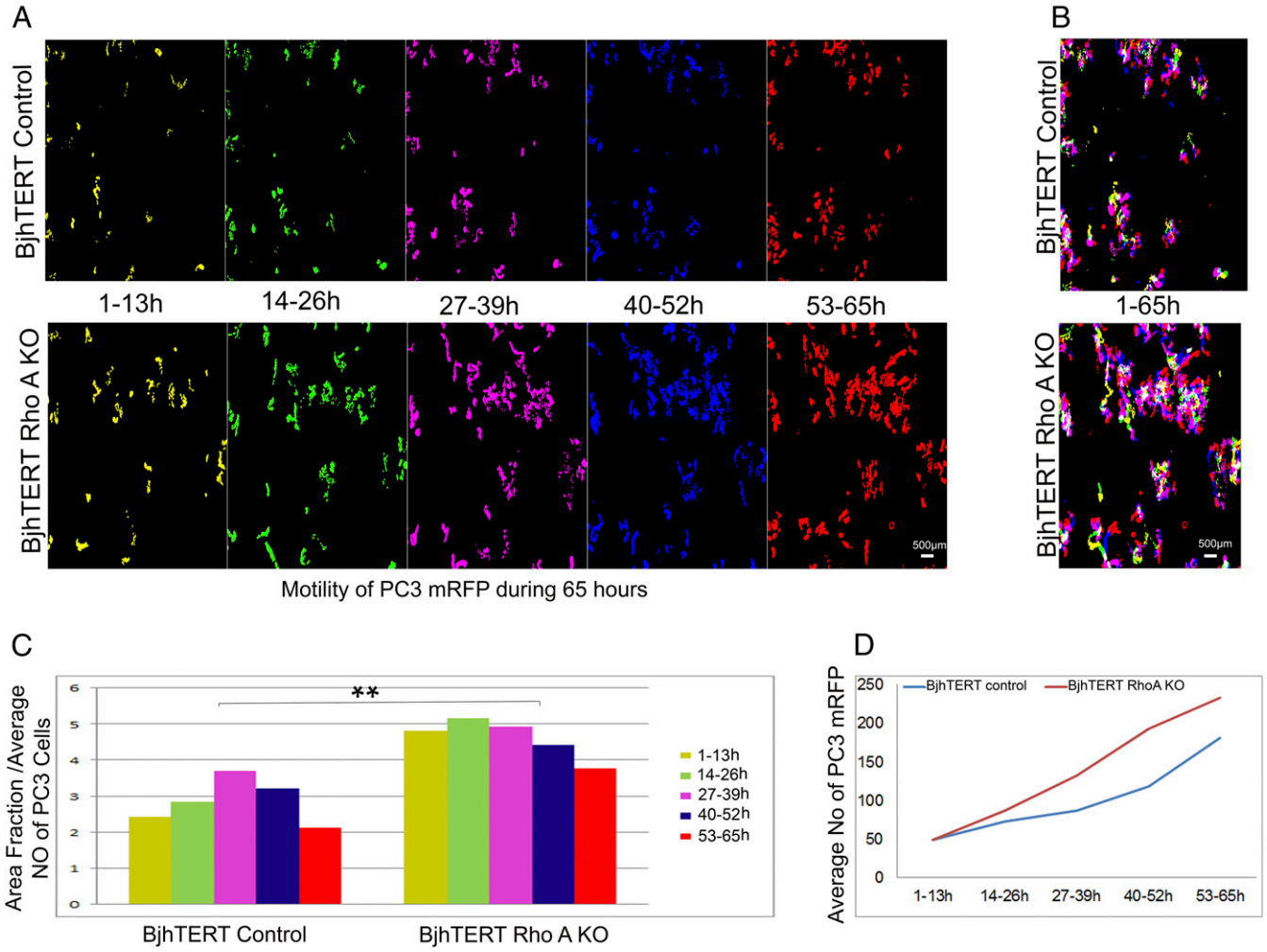

Fig. 2. RhoA-KO fibroblasts induce tumor-cell motility and proliferation. Live-cell TIRF microscopy imaging. (*A*) Trajectories of PC3 mRFP prostate cancer cells during 13-h intervals. Color-coded images show a 65-h time-point projection of the red-labeled tumor cells: yellow (1–13 h), green (14–26 h), magenta (27–39 h), blue (40–52 h), and red (53–65 h). (*B*) Maximum projection of all five color-coded images showing the total motility (full trajectories) of the PC3 mRFP tumor cells over the 65 h. (*C*) Kinetics of tumor-cell motility. Motility of tumor cells quantified by calculation of the areas of the cell trajectories, normalized for mean number of cells in each 13-h interval. $^{**}P = 0.0037$. (*D*) Mean number of PC3 mRFP cells that proliferated during each 13-h interval (of five time points). See also Movies S1 and S2.

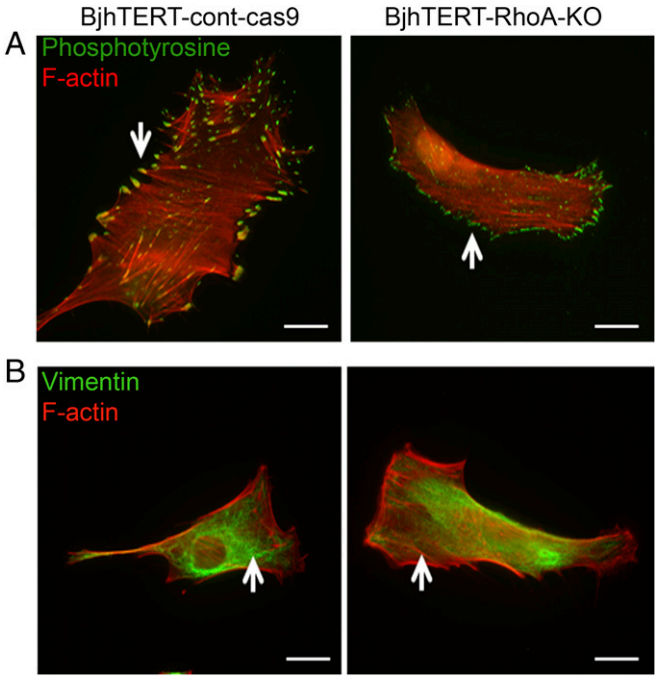

Fig. 3. RhoA-KO fibroblasts show altered cytoskeletal organization and cell-matrix adhesion. Representative images showing phosphotyrosine (pY) (green) (*A*), vimentin (*B*), and F-actin (red) (*A* and *B*) in the control and RhoA-KO fibroblasts (as indicated). Images are representative of at least three independent experiments. Arrows indicate large focal adhesions linked to stress fibers (*A*) and the spatial organization of the vimentin filaments (*B*). (Scale bars, 20 μm.)

Coculture of RhoA-KO Fibroblasts with Cancer Cells Activates Proinflammatory Genes and Rho-Related Pathway Activity. To identify factors that might mediate the tumor promoting effects of RhoA-KO fibroblasts, gene-expression analysis was performed for RhoA-KO fibroblasts and PC3 mRFP prostate cancer cells before coculturing and after 6 d of coculturing, using the Affymetrix Whole Transcript Assay platform and validation of selected genes using the qPCR technique on newly generated samples.

After coculture with PC3 mRFP cells, the RhoA-KO fibroblasts manifested higher expression levels of such proinflammatory signature genes as *IL-1A*, *IL-1B*, *IL-6*, *IL-8*, chemokine (C-C motif) ligand 2 (*CCL2*), and TNF-α–induced protein 2 (*TNFAIP2*) (Table S1) (10, 21). In contrast, in the control fibroblasts expression of genes for proinflammatory cytokines did not seem to change after the coculturing. In turn, the PC3 cells that were cocultured with RhoA-KO fibroblasts exhibited higher expression of certain genes of proinflammatory signature (*IL-6*, *IL-8*, and *CCL2*) (Table S2), compared with the PC3 cells cocultured with control fibroblasts.

To increase the power of our analysis, we further applied the network enrichment analysis (NEA) (22). Similarly to the gene-set enrichment analysis of differential expression (DE), NEA can summarize observations by raising them to the pathway level. However, it is more powerful than the former method because of considering network connections between differentially expressed and pathway genes, so that the latter may be identified even when their own expression is not changed (23).

Both the control and RhoA-KO fibroblasts were sampled before and after coculturing with the PC3 prostate cancer cells. Using Venn diagram sampling and NEA tools available at https://www.evinet.org, we created lists of genes that were differentially expressed between the control and RhoA-KO fibroblasts as measured before (Datasets S1 and S2) and after (Datasets S3 and S4), or both before and after (Datasets S5 and S6) coculturing them with the PC3 cells. Separating DE genes into up- and down-regulated fractions produced six gene lists in total. Unexpectedly, the "up" and "down" gene lists specifically before the coculturing (Fig. 5, UP_BEFORE, DOWN_BEFORE) did not manifest any significant network connections toward Rho signaling pathways. Remarkably though, the latter pathways appeared significantly connected to a set of 55 genes that were consistently up-regulated with the fibroblast and cancer cell coculturing (Fig. 5, UP_BOTH). Similarly, the Rho pathways were enriched in connections to the gene sets specifically up-regulated and down-regulated following the coculturing (Fig. 5, UP_AFTER, DOWN_AFTER). As an example, we looked at details of functional connections with the mDia-SRF pathway, which is known for its involvement in actin modifications and thus appeared potentially implicated in the consequences of our RhoA KO. At the gene-expression level, we observed that neither serum response factor (SRF) nor other relevant genes were altered because of the knockout. However, in network enrichment analysis this pathway functionally linked to the UP_BOTH, UP_AFTER, and DOWN_AFTER lists (Fig. 5). We could see that the most central, significantly linked gene was SRF itself, with a potential

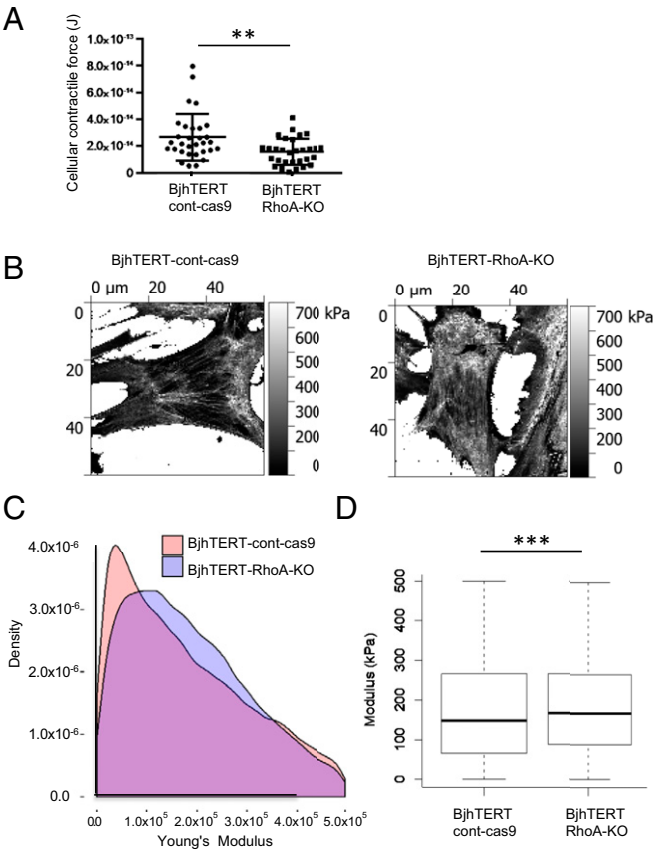

Fig. 4. Altered cellular contractile forces and cell stiffness of tumor-stimulatory fibroblasts. (*A*) Contractile forces of individual control (dots) and RhoA-KO (squares) fibroblasts. The *P* value indicates a difference of 0.004. $^{**}P > 0.01$. (*B*) Image showing the Young's modulus of the locations over the control (*Left*) and RhoA-KO (*Right*) fibroblasts. Lighter colors indicate higher modulus. (*C*) Density plot showing distribution of the measured stiffness for values of individual locations of measurement within the physiological range of 0 kPa to 75 kPa, for 33,505 data points from control fibroblasts, and 33,505 data points from RhoA-KO fibroblasts. (*D*) Boxplot showing distributions and median values of measured stiffness for values within the physiological range of 0 kPa to 75 kPa, including 33,505 data points for control fibroblasts, and 33,505 data points for RhoA-KO fibroblasts. Data for the RhoA-KO cells show significantly higher stiffness. $^{***}P < 2.2e\text{-}16$.

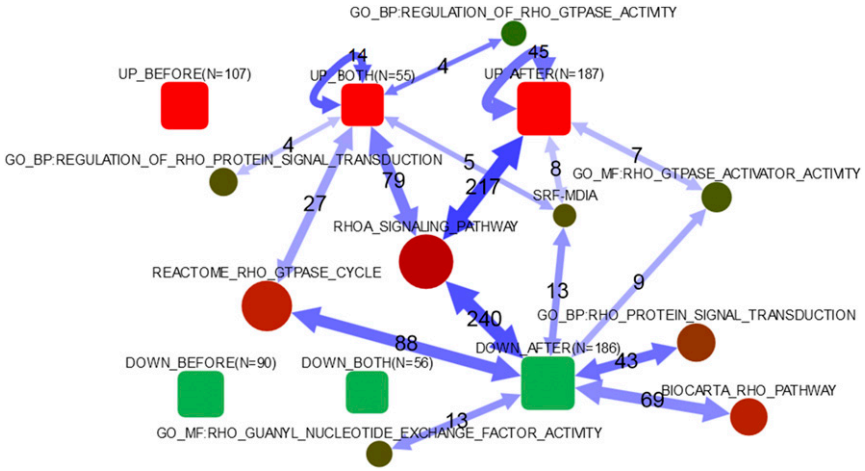

Fig. 5. Network enrichment of differentially expressed genes in pathways related to RhoA regulation. Global patterns in regard to pathways related to Rho signaling. Connectivity between DE lists and individual genes of the SRF–mDia pathway. Rounded boxes: lists of differentially expressed genes; AFTER, after coculturing; BEFORE, before coculturing; BOTH, both before and after coculturing; DOWN, down-regulation because of RhoA knock-out of ≥twofold; N, number of genes in list; UP, up-regulation due to RhoA KO of ≥ twofold. Circles: pathways; the size reflects the number of member genes, the color indicates the relative activity in the global network (total number of links). Double-headed arrows summarize individual gene–gene connections (in either direction, and undirected ones) in the global network between any differentially expressed genes and any pathway members. Numeric labels give numbers of individual gene–gene network connections behind the arrows. Only arrows corresponding to significant network enrichment are shown (adjusted $P < 0.05$). The lists of the genes in each group are given in Datasets S1–S6. The data on the SRF–mDia pathway are shown as described previously (24, 25).

involvement of the other genes presented by Gopinath et al. (24) and Geneste et al. (25).

Our observations suggest that the Rho-related transcriptome changes caused by the RhoA KO emerged mainly during the coculturing with the tumor cells rather than preexisting in the fibroblasts before this procedure (i.e., in the PC3-naive fibroblasts).

RhoA-KO Fibroblasts Support a Growth Pattern of Compact Tumor Clusters and Cell Contacts in 3D Collagen Cocultures. To understand how the changes in the fibroblast Rho pathways, gene-expression programs, contact-dependent neighbor suppression, and cytoskeleton that were induced by the RhoA KO and coculturing in vitro relate to the increased PC3 tumorigenesis in vivo, we established a 3D coculture model of the BjhTERT fibroblasts and PC3 mRFP prostate cancer cells. Equal numbers of control (BjhTERT cont-cas9) and RhoA-KO fibroblasts alone or in combination with PC3 mRFP cells were embedded in the 3D collagen matrix and (co)cultured for 7 d. In the 3D monocultures, control fibroblasts formed dense cross-networks with branching and elongated sprouting. Consistent with the cytoskeletal changes in 2D cultures, for RhoA-KO fibroblast 3D monocultures, fluorescence imaging of filamentous actin revealed impaired stress fibers in conjunction with less sprouting, as a blunt-ended phenotype (Fig. 6*A*). In the cocultures for RhoA-KO fibroblasts, the PC3 mRFP cells grew in clusters surrounded by these fibroblasts, and showed compact positioning of their nuclei, whereas both PC3 cells and fibroblasts were more dispersed in the control fibroblast cocultures (Fig. 6*B*). To quantify this compactness versus dispersal of PC3 tumor cells in the fibroblast cocultures, we generated a "Clustering Index." PC3 cells cocultured with RhoA-KO fibroblasts had a significantly higher Clustering Index compared with PC3-cell and control-fibroblast cocultures (Fig. 6*C*). These results suggest that by driving actin-cytoskeleton–dependent fibroblast branching, RhoA signaling can support coincident dispersal of the cocultured tumor cells. Therefore, in the 3D microenvironment, RhoA ablation in fibroblasts can promote the delayed tumor growth by supporting tumor-cell survival and stem-like properties via cell–cell contacts, altered Rho pathways, and interactions with (or the close distance of) the fibroblasts with increasing chemokine production (i.e., by mechanical and biochemical mechanisms).

Discussion

Although interactions between a tumor and the stroma are regulated by various biochemical reactions, it is becoming increasingly clear that mechanical cues also have a significant role in these interactions (26). In the present study, we have shown that these RhoA-KO fibroblasts that are characterized by altered gene-expression profile, cytoskeleton, and mechanical properties can promote tumor growth, although they do not show common markers of CAFs.

Indeed, our experimental model was different from any other model that studied CAFs. Here, we show that normal inhibitory fibroblasts can be switched into a promoting subtype before they become CAFs by the classic definition. Our cells showed that RhoA ablation had an immediate "net effect" on the interaction between fibroblasts and cancer cells. In other words, this effect of fibroblasts apparently was not induced by the cells' coexistence and coevolution during extended time periods.

Here, we investigated the proliferation and migration of the metastatic PC3 prostate cancer cell line in cocultures with fibroblasts in vitro and in a subcutaneous tumor xenograft model in mice. A loss of the tumor-inhibitory capacity of these fibroblasts upon RhoA ablation was observed in these 2D systems and in the xenograft tumors. Interestingly, in the presence of RhoA-KO fibroblasts in the 3D collagen system, the PC3 tumor cells formed colonies that were prominently compact clusters with closely positioned nuclei. This might be the underlying cause of the growth of the tumor xenografts in this study, whereby the tumor cells coinjected with RhoA-KO fibroblasts started to grow after a long lag-phase, to form subcutaneous tumors. We suggest that the cluster-like aggregation and ample homotypic cancer-cell contacts in the presence of RhoA-KO fibroblasts in this 3D system are linked to the tumor propagating and stem-like properties. Furthermore, in the in vivo xenograft model, low numbers of tumor cells were enough to initiate tumor growth when they were in the presence of RhoA-KO fibroblasts, with

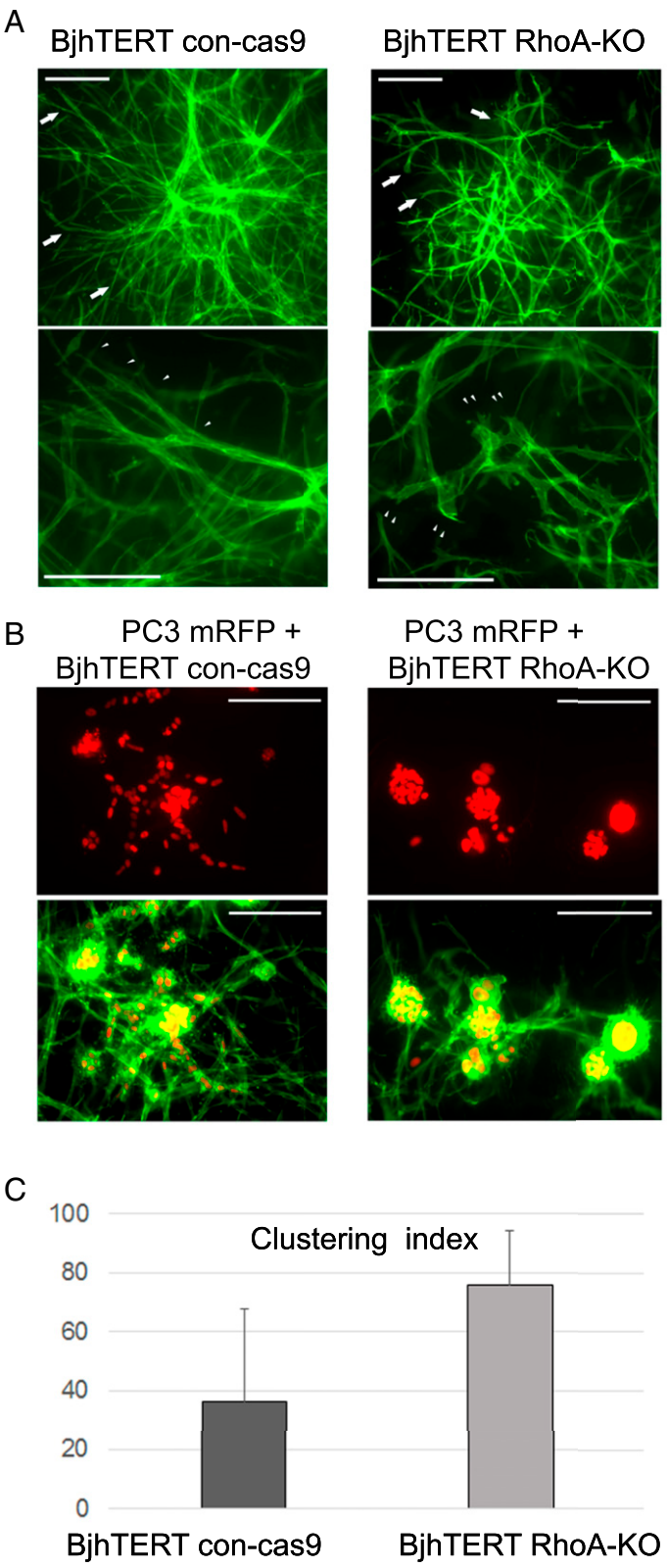

Fig. 6. Growth of PC3 tumor cells with RhoA-KO fibroblasts in 3D collagen. (*A*) Phenotypes of control (cont-cas9) and RhoA-KO BjhTERT fibroblasts cultured for 7 d in the 3D type I collagen matrix. Arrows indicate differences in sprouting ability between control and RhoA-KO fibroblasts. Higher magnifications and arrowheads indicate elongated sprouting in control compared with RhoA-KO fibroblasts with the blunt-ended phenotype. (*B*) To assess growth of PC3 tumor cells with RhoA-KO fibroblasts in 3D collagen, equal numbers of PC3mRFP cells and BjhTERT control or RhoA-KO fibroblasts were suspended as single cells into 3D collagen and cultured for 7 d. (*C*) Clustering Index calculated to quantify the spreading and compactness of growth of PC3 tumor spheres in coculture with RhoA-KO fibroblasts. For the Clustering Index, the number of sprouting growths was calculated (total n = 16 image fields from two independent repeats) and subtracted from a constant value: Clustering Index = [20 − (mean number of sprouting growths)] ×5. (Scale bars, 200 μm.)

the emergence of palpable tumors delayed, both of which are known hallmarks of tumor-propagating cells.

Our findings indicate that upon coculturing, the transcriptomes of both the RhoA-KO fibroblasts and the tumor cells are shaped by activation of the proinflammatory signature. It is known that inflammation promotes cancer growth and metastasis (27, 28). Thus, this RhoA KO might provide a link between inflammation and cancer via the induction of a proinflammatory environment. The observed increase of tumor-cell motility in the presence of the RhoA-KO fibroblasts is in line with previous observations that proinflammatory chemokines can promote tumor-cell migration (27). In addition, the increased PC3 cell motility appears to be because of the present finding that upon RhoA loss, these RhoA-KO fibroblasts lose their contact-dependent neighbor-suppression effects.

The observed RhoA-mediated orchestration of many different biochemical and physical factors makes RhoA a "master-regulator" of interactions between tumors and stroma (26). Cytoskeletal filaments in the cell can convert mechanical signals into biochemical signals via the mechano-sensitive proteins of the cell. In this way, the extracellular and intracellular mechanical properties of the cells can activate different downstream processes, such as cell migration, adhesion, gene transcription, and differentiation (29). Furthermore, these RhoA-KO tumor-promoting fibroblasts showed significant reduction in α-SMA expression. Such concordant down-regulation can be explained via the regulation of smooth muscle cell-specific promoter activity of the α-SMA gene through RhoA signaling (30).

We observed that the RhoA-KO fibroblasts showed increased homogeneous stiffness, with fewer soft locations, and decreased contractile forces. This is in line with the previous observations that RhoA is a key regulator of the mechanical properties of fibroblasts (31–33). These mechanical changes in the RhoA-KO fibroblasts were linked to the loss of wide stress fibers and large focal adhesions. De Wever et al. proposed that fibroblasts in the tumor microenvironment can behave as particularly motile units, which can invade the cancer-cell compartment (34), potentially because of the altered cytoskeleton of these cells (35). In line with the mechanical control of tumor growth by fibroblasts in the tumor microenvironment, Kumar and Weaver suggested that mechanical forces have a major role in the onset and progression of cancers (5). In addition, based on the literature in the field, Karagiannis et al. proposed a working model for how mechanical and adhesive properties of fibroblasts govern local cancer growth (36 and references therein). In their model, the fibroblasts in tumors show altered cell-matrix adhesion, increased migration, and changed mechanics, which might stimulate cancer cells to migrate toward stromal regions that are less dense, and thereby increase the size of a tumor. Moreover, cell-matrix stiffness has been shown to stimulate cytokinesis, which suggests that the increased stiffness of the surrounding fibroblasts can also stimulate the proliferation of cancer cells (37). These ideas are in line with our findings that these RhoA-KO tumor-promoting fibroblasts showed increased homogeneous stiffness and fewer soft locations, with altered cytoskeleton and cell-matrix adhesion.

Tumor cells go through many changes, both phenotypically and genetically, as they pass through the different stages of initiation, growth, invasion, colonization, and metastasis. This might be true for the fibroblasts in the tumor microenvironment

too. As we have shown here, the mere RhoA KO do not yet turn normal fibroblasts into full-scale CAFs, even though their phenotype shifts from inhibitory to noninhibitory and then into tumor-promoting cells. Thus, although not being classic CAFs, the fibroblasts acquired key properties that proved to be sufficient for promotion of tumor-cell growth.

The loss of α-SMA and reduction of contractile forces in these RhoA-KO fibroblasts was another difference from CAFs. Therefore, they might respond differently to certain signals, including RhoA signaling. Importantly, we found that knocking out RhoA in normal fibroblasts did not activate significant relations to the Rho signaling pathway until these fibroblasts met the tumor cells. This might be highly relevant in the context of tumor initiation and early development.

We have demonstrated that fibroblasts with ablated RhoA lose their normal inhibitory capacity in vitro, induce tumor growth in vivo and migration and proliferation of tumor cells in vitro, and support clustering of cocultured tumor cells in a 3D system. In the light of these results, RhoA appears to be an important regulator of the switch from tumor-inhibitory to tumor-promoting fibroblasts. The regulatory effects on tumor-cell growth must be imposed via a complex course of mechanical and biochemical reactions. An aspect here that remains elusive to the scope of the present study is how the loss of RhoA (which alters the mechanical and biochemical properties of normal stromal fibroblasts) can trigger a stem-like phenotype in these PC3 prostate cancer cells. Probably, increased level of proinflammatory genes plays role in inducing the expression of stemness-related properties of tumor cells (38, 39). We have demonstrated that loss of RhoA changed the cytoskeleton, the contractile forces and cell stiffness of the cells, induced a proinflammatory state, and interfered with Rho signaling cascades. However, further studies are needed to determine if the RhoA levels in stromal fibroblast govern the carcinoma aggressiveness and the clinical outcome.

Conclusions

Our findings suggest that RhoA controls the tumor-inhibitory capacity of fibroblasts through their mechanical properties and biochemical signaling. It also appears that a significant part of the RhoA-dependent signaling is activated by the presence of these tumor cells. A more detailed identification of the molecular mechanisms that underlie this intercellular control is a promising area for future studies.

Materials and Methods

RhoA CRISPR/Cas and Lentivirus System. We prepared lentiviral CRISPR/Cas9 vectors that coexpressed *Streptococcus pyogenes* Cas9, PuroR, and a human U6 promoter driving expression of anti-RhoA guideRNAs (40). The gene-specific regions of the guideRNA sequences were designed by the CRISPR design tool from the Zhang laboratory (crispr.mit.edu/), and their sequences were: RhoA_1, GAACTATGTGGCAGATATCG; RhoA_2, GACAGCCCTGATAGTTT; and RhoA_3, GCTGCCATCCGGAAGAAAC. The lentiviruses were generated using standard third-generation packaging vectors in 293T cells. In addition, we constructed an empty lentiviral control vector.

Established RhoA KO BjhTERT Fibroblast Line. We transduced three BjhTERT clones of different origin: BjhTERT (original), BjhTERT-C (crossy), and BjhTERT-W (whirly) (6), with the RhoA lentiviral CRISPR/Cas9 vector. A mixture of the three vectors (i.e., RhoA_1, RhoA_2, and RhoA_3) was used to transduce the fibroblasts in the presence of Polybrene. In parallel to the KO line, a negative control BjhTERT fibroblast line was generated using the empty lentiviral vector. The cells were selected with 2 μg/mL puromycin. A polyclonal line was collected and subcultured, and the status of RhoA at the protein level was evaluated using Western blotting.

RT-PCR Analysis. Quantitative real-time PCR protocol is described in *SI Materials and Methods*. qPCR data were analyzed using the reference genes TBP. Each reaction was repeated three times.

Ct values were determined for the internal control (glyceraldehyde-3-phosphate dehydrogenase or TATA-binding protein) and for the test genes at the same threshold level in the exponential phase of the PCR curves. Relative quantification [comparative Ct (ΔΔCt) method] was used to compare the expression level of the test genes with the internal control. Dissociation curve analysis was performed after every run to check the specificity of the reaction.

Western Blotting. Anti-RhoA antibody (Cat. no. sc-418; Santa Cruz Biotechnology) and anti–α-SMA antibody (Cat. no. M0851; Dako) were used. The protocol is described in *SI Materials and Methods*.

Tumor-Inhibitory Capacity Assay. Tumor-cell proliferation on fibroblast monolayers was analyzed in 384-well plates. Fibroblasts were plated in 100 μL cell-culture medium [IMDM; 10% (vol/vol) FBS, PSG] and cultured for 5 d, during which time they formed confluent monolayers. After the formation of full confluent monolayers, 80 μL medium was removed and 200 H2AmRFP-labeled PC3 prostate cancer cells (PC3 mRFP cells) were plated on top of the fibroblast monolayers in 80 μL cell-culture medium. The control wells contained 200 labeled tumor cells without the fibroblast monolayers.

Microscopy, Image Analysis, and Quantification. Immunofluorescence microscopy, automatic microscopy, and analysis of the tumor-cell numbers were carried out at the single-cell level using an automated microscope system, as previously described (6, 41, 42).

Coinjection of Tumor Cells and Fibroblasts in SCID and SCID-Beige Mice. A nontumorigenic number of PC3 prostate cancer cells (2×10^4 cells) (43, 44) were injected subcutaneously alone or when mixed with fibroblasts (1×10^6 cells) into 4-wk-old female SCID or SCID-beige mice (Taconik). Each mouse received one injection. The occurrence and growth of tumors were then analyzed up to 80-d postinjection. The procedures using the SCID and SCID-beige mice were approved by the North Stockholm Ethical Committee (Decision no. 192/14). Ten mice were used for the experiments. The mice were monitored for tumor growth twice a week, with the tumors measured using a caliper (mm^3).

TIRF Microscopy Live-Cell Motility Assay. Fibroblasts were seeded into six-well plates, with 70,000 BjhTERT control or BjhTERT RhoA-KO fibroblasts cultured in each well, for 18–24 h. Each fibroblast culture was cocultured with 5,000 PC3 mRFP prostate cancer cells, with the coculture then kept in the incubator for another 24 h. The next day, each well was washed and supplemented with fresh medium. The plates were then relocated to the TIRF microscope incubation chamber, at constant 37 °C and under 5% (vol/vol) CO_2. The ZEN2 Software was used to design the experiment and guided the complete microscopic unit automatically. The time-lapse imaging was recorded for 65 h, with a 1-h interval per capture. A field of 25 images (5 × 5) that covered a total area of 4.118 × 3.085 mm^2 was captured using the 10× objective lens.

Three-Dimensional Growth Assays. Collagen matrix was prepared by dissolving rat-tail collagen I (Sigma-Aldrich) in 0.3% acetic acid, with this neutralized with NaOH and diluted to a final concentration of 2.25 mg/mL in MEM on ice (45). Single-cell suspensions of 5,000 H2AmRFP-plasmid expressing PC-3 cells and 5,000 control or RhoA-KO fibroblasts were prepared in IMDM supplemented with 10% (vol/vol) FBS, GlutaMAX (Gibco), and 100 U/mL penicillin-streptomycin. The cells were rapidly mixed with collagen gels and casted in 48-well plates (Nunclon Delta Surface, Thermo Scientific). The cultures were incubated in an incubator at 37 °C and 5% (vol/vol) CO_2 for 7 d and fixed with 4% (vol/vol) PFA for 1 h at room temperature. Three-dimensional matrices were stained with phalloidin-Alexa488 to analyze PC-3 sphere growth and mounted into Vectashield reagent for imaging with a Zeiss AxioImager.Z2 upright epifluorescence microscope. *Z*-stacks were imaged with the 10× objective (EC Plan Neofluar, NA 0.3) using a digital camera (Hamamatsu Orca Flash 4.0 LT). Images were processed with ZEN 2 pro software (Zeiss) using extended depth-of-focus module (contrast function; *z*-stack alignment: highest; contrast length scale 7; smoothing 11; reconstruction 0.15) for sharply extracting *z*-stacks for image quantification using the ImageJ software. The growth of the PC3 tumor cell spheres was analyzed and the Clustering Index was calculated to quantify the nonspreading, compact growth of the PC3 tumor spheres in coculture with RhoA-KO fibroblasts. For the Clustering Index, the level of sprouting was calculated (total $n = 16$ image fields, from two independent repeats) and subtracted from a constant value: Clustering Index = [20 − (mean number of sprouting growths)] ×5.

Atomic Force Microscopy. Atomic force microscopy imaging was performed using a JPK Nanowizard 3 system installed on an inverted optical microscope (Nikon TE-1). The system was fitted with a Petri dish heater that held the cell-culture

dishes in a 37 °C. Advanced QI Mode provided the possibility to rapidly collect maps of approach-retract cycles (force curves) across the samples, from which mechanical maps were constructed (46). Atomic force microscopy has a lateral range of 100 μm and a vertical range of 15 μm, which is easily sufficient to characterize the cells used in this study. A standard contact mode cantilever (Bruker MLCT-E; nominal spring constant, 0.1 nm^{-1}; resonance frequency, 50 kHz; tip radius, 20 nm) was calibrated in air before the measurements, by first measuring the deflection sensitivity (nm/V) against a stiff polystyrene substrate, and then fitting the fundamental resonance peak in the thermal noise spectrum to determine the spring constant (47). This relatively stiff cantilever was chosen to minimize the effects of bulk hydrodynamic drag, while being soft enough to register differences in force and provide sufficiently large indentations (hundreds of nanometers) that the cytoskeleton controlled the stiffness. The cell dish was placed in the Petri dish heater, and the head placed over it. Before acquiring images, the deflection sensitivity was measured against a bare Petri dish with medium. Image resolution was 128 × 128 pixels. Approach and retract distances were set to 1.5 μm, and the speed was set to 50 μm s^{-1}. At this speed and resolution, the acquisition time was around 20 min per image.

Each interaction can be considered as an indentation experiment from which the effective Young's modulus can be extracted (JPK Data Processing software). The approach curve was first corrected for baseline position and slope, and converted to force versus separation. The Hertz model was then performed using square pyramidal indenter geometry, with an average edge angle of 25°. A batch process was used to fit the 128 × 128 indentation plots after optimizing the fitting parameters on a representative selection of the data. Apart from the Young's modulus, the contact position was also determined via this fitting procedure (i.e., the height at which the fit to the cantilever deflection deviated from zero).

Further image handling was performed in Gwyddion (gwyddion.net). Modulus histograms for each image were prepared using 246 bins. Graphs were prepared in Origin (OriginLab). There was a large variation between cells, and one image of each cell shows the qualitative difference in stiffness distribution over the cell (Fig. S6).

Traction Force Microscopy. Traction force microscopy calculations were performed as previously described (48). A description may also be found in *SI Materials and Methods*.

Affymetrix Microarrays. Four-day-old fibroblast monolayers were cocultured with the PC3 mRFP prostate tumor cells, plated at a ratio of 1:30 according to the number of plated fibroblasts. After 6 d of coculturing, the cells were sorted by fluorescence-activated cell sorting. The total RNA was isolated from monocultured and cocultured cells using kits. Then, 150 ng total RNA was used for the transcriptomic analysis.

Array hybridization, washing, staining, and scanning were performed using the Affymetrix WT Plus labeling and hyb to the HG 2.1 ST Array plate. Summary, normalization, and background correction were performed in Affymetrix Expression Console (v1.3.1) using the robust multiarray average method. The GEO accession number for the Affymetrix data is GSE83913 and available at www.ncbi.nlm.nih.gov/geo/query/acc.cgi?acc=GSE83913.

Differential Expression Analysis. We compared expression in the following contrasts of our interest: (*i*) BjhTERT before confrontation (control) vs. BjhTERT before confrontation (knock-out); (*ii*) BjhTERT after confrontation (control) vs. BjhTERT after confrontation (knock-out); and (*iii*) PC3 after confrontation (control) vs. PC3 after confrontation (knock-out).

To increase confidence, we calculated fold-change values by using both the wild-type control and the empty vector control as substitutes for biological replicates.

For the NEA, we selected genes with twofold change in either direction the "up" and "down" lists were treated separately. Fold-change values were calculated as arithmetic differences between the log-transformed Affymetrix expression values obtained at the processing steps described in section "Affymetrix microarrays" above.

Network Enrichment Analysis. As there were not enough replicated samples for a detailed differentially expressed analysis at the level of the individual genes, we used a new method of NEA (22) that estimates pathway enrichment in differentially expressed gene lists in a more robust manner (49) compared with both single-gene differential expression and the state-of-the-art gene-set enrichment analysis (50).

NEA evaluates the network connectivity between experimentally defined gene sets and some previously known or hypothesized gene sets with a clearly defined function. The individual connections are edges (functional links) in the global network between any of the genes of the former and latter gene sets. As even spurious connections between random gene sets can be found in a dense network, the significance of each pattern is evaluated using a special algorithm (22, 23).

The three components required for the network enrichment analysis were provided as follows: (*i*) experimental gene sets that were created as differentially expressed gene lists by comparing mRNA expression in KO cells with that in both of the controls, before and after coculturing with the cancer cells; (*ii*) functional genes sets (pathways of Gene Ontology terms); and (*iii*) a global network of physical interactions and other functional coupling between genes and proteins that was created from a multifaceted data integration of high-throughput and curated resources, as described in ref. 51. The current version included 19,027 genes (mapped to HUGO gene symbols) with 947,000 links that connected them.

ACKNOWLEDGMENTS. This study was supported by grants from the Swedish Research Council and the Swedish Cancer Society. Bioinformatics support from National Bioinformatics Infrastructure Sweden is gratefully acknowledged. A.K.B.G. was supported by the Syskonen Svenssons Foundation and Ollie and Elof Ericssons Foundation. T.P., V.K., and H.G. were supported by fellowships by a matching grant jointly awarded by the Concern Foundation, Los Angeles, and the Cancer Research Institute, New York. A.A. was supported by Emil och Wera Cornells Stiftelse. R.J.L. was supported by the Dutch Cancer Society Grant UU 2012-5667.

1. Donjacour AA, Cunha GR (1991) Stromal regulation of epithelial function. *Cancer Treat Res* 53:335–364.
2. Kenny PA, Bissell MJ (2003) Tumor reversion: Correction of malignant behavior by microenvironmental cues. *Int J Cancer* 107(5):688–695.
3. Mintz B, Illmensee K (1975) Normal genetically mosaic mice produced from malignant teratocarcinoma cells. *Proc Natl Acad Sci USA* 72(9):3585–3589.
4. Rønnov-Jessen L, Petersen OW, Bissell MJ (1996) Cellular changes involved in conversion of normal to malignant breast: Importance of the stromal reaction. *Physiol Rev* 76(1):69–125.
5. Kumar S, Weaver VM (2009) Mechanics, malignancy, and metastasis: The force journey of a tumor cell. *Cancer Metastasis Rev* 28(1-2):113–127.
6. Flaberg E, et al. (2012) The architecture of fibroblast monolayers of different origin differentially influences tumor cell growth. *Int J Cancer* 131(10):2274–2283.
7. Stoker MG, Shearer M, O'Neill C (1966) Growth inhibition of polyoma-transformed cells by contact with static normal fibroblasts. *J Cell Sci* 1(3):297–310.
8. Alkasalias T, et al. (2014) Inhibition of tumor cell proliferation and motility by fibroblasts is both contact and soluble factor dependent. *Proc Natl Acad Sci USA* 111(48):17188–17193.
9. Olumi AF, et al. (1999) Carcinoma-associated fibroblasts direct tumor progression of initiated human prostatic epithelium. *Cancer Res* 59(19):5002–5011.
10. Raz Y, Erez N (2013) An inflammatory vicious cycle: Fibroblasts and immune cell recruitment in cancer. *Exp Cell Res* 319(11):1596–1603.
11. Kalluri R, Zeisberg M (2006) Fibroblasts in cancer. *Nat Rev Cancer* 6(5):392–401.
12. Mogilner A, Keren K (2009) The shape of motile cells. *Curr Biol* 19(17):R762–R771.
13. Arthur WT, Noren NK, Burridge K (2002) Regulation of Rho family GTPases by cell-cell and cell-matrix adhesion. *Biol Res* 35(2):239–246.
14. Lessey EC, Guilluy C, Burridge K (2012) From mechanical force to RhoA activation. *Biochemistry* 51(38):7420–7432.
15. Bozoky B, et al. (2013) Novel signatures of cancer-associated fibroblasts. *Int J Cancer* 133(2):286–293.
16. Zhou Y, et al. (2013) Inhibition of mechanosensitive signaling in myofibroblasts ameliorates experimental pulmonary fibrosis. *J Clin Invest* 123(3):1096–1108.
17. Zhao XH, et al. (2007) Force activates smooth muscle alpha-actin promoter activity through the Rho signaling pathway. *J Cell Sci* 120(Pt 10):1801–1809.
18. Mullin BH, Mamotte C, Prince RL, Wilson SG (2014) Influence of ARHGEF3 and RHOA knockdown on ACTA2 and other genes in osteoblasts and osteoclasts. *PLoS One* 9(5):e98116.
19. Huang X, et al. (2012) Matrix stiffness-induced myofibroblast differentiation is mediated by intrinsic mechanotransduction. *Am J Respir Cell Mol Biol* 47(3):340–348.
20. Calvo F, et al. (2013) Mechanotransduction and YAP-dependent matrix remodelling is required for the generation and maintenance of cancer-associated fibroblasts. *Nat Cell Biol* 15(6):637–646.
21. Mookherjee N, et al. (2006) Modulation of the TLR-mediated inflammatory response by the endogenous human host defense peptide LL-37. *J Immunol* 176(4):2455–2464.
22. Alexeyenko A, et al. (2012) Network enrichment analysis: Extension of gene-set enrichment analysis to gene networks. *BMC Bioinformatics* 13:226.
23. Alexeyenko A, et al. (2015) Confrontation of fibroblasts with cancer cells in vitro: Gene network analysis of transcriptome changes and differential capacity to inhibit tumor growth. *J Exp Clin Cancer Res* 34:62.
24. Gopinath SD, Narumiya S, Dhawan J (2007) The RhoA effector mDiaphanous regulates MyoD expression and cell cycle progression via SRF-dependent and SRF-independent pathways. *J Cell Sci* 120(Pt 17):3086–3098.

25. Geneste O, Copeland JW, Treisman R (2002) LIM kinase and Diaphanous cooperate to regulate serum response factor and actin dynamics. *J Cell Biol* 157(5):831–838.
26. Stachowiak MR, et al. (2014) A mechanical-biochemical feedback loop regulates remodeling in the actin cytoskeleton. *Proc Natl Acad Sci USA* 111(49):17528–17533.
27. Sun Y, et al. (2015) Pro-inflammatory cytokine IL-1β up-regulates CXC chemokine receptor 4 via Notch and ERK signaling pathways in tongue squamous cell carcinoma. *PLoS One* 10(7):e0132677.
28. Erez N, Truitt M, Olson P, Arron ST, Hanahan D (2010) Cancer-associated fibroblasts are activated in incipient neoplasia to orchestrate tumor-promoting inflammation in an NF-kappaB-dependent manner. *Cancer Cell* 17(2):135–147.
29. Hoffman BD, Grashoff C, Schwartz MA (2011) Dynamic molecular processes mediate cellular mechanotransduction. *Nature* 475(7356):316–323.
30. Mack CP, Somlyo AV, Hautmann M, Somlyo AP, Owens GK (2001) Smooth muscle differentiation marker gene expression is regulated by RhoA-mediated actin polymerization. *J Biol Chem* 276(1):341–347.
31. Chrzanowska-Wodnicka M, Burridge K (1996) Rho-stimulated contractility drives the formation of stress fibers and focal adhesions. *J Cell Biol* 133(6):1403–1415.
32. Gad AKB, et al. (2012) Rho GTPases link cellular contractile force to the density and distribution of nanoscale adhesions. *FASEB J* 26(6):2374–2382.
33. Jatho A, et al. (2015) RhoA ambivalently controls prominent myofibroblast characteritics by involving distinct signaling routes. *PLoS One* 10(10):e0137519.
34. De Wever O, Demetter P, Mareel M, Bracke M (2008) Stromal myofibroblasts are drivers of invasive cancer growth. *Int J Cancer* 123(10):2229–2238.
35. De Wever O, et al. (2004) Critical role of N-cadherin in myofibroblast invasion and migration in vitro stimulated by colon-cancer-cell-derived TGF-beta or wounding. *J Cell Sci* 117(Pt 20):4691–4703.
36. Karagiannis GS, et al. (2012) Cancer-associated fibroblasts drive the progression of metastasis through both paracrine and mechanical pressure on cancer tissue. *Mol Cancer Res* 10(11):1403–1418.
37. Sambandamoorthy S, et al. (2015) Matrix compliance and the regulation of cytokinesis. *Biol Open* 4(7):885–892.
38. Avnet S, et al. (November 26, 2016) Cancer-associated mesenchymal stroma fosters the stemness of osteosarcoma cells in response to intratumoral acidosis via NF-κB acivation. *Int J Cancer*, 10.1002/ijc.30540.
39. Chang TS, et al. (2016) Inflammation promotes expression of stemness-related properties in HBV-related hepatocellular carcinoma. *PLoS One* 11(2):e0149897.
40. van de Weijer ML, et al. (2014) A high-coverage shRNA screen identifies TMEM129 as an E3 ligase involved in ER-associated protein degradation. *Nat Commun* 5:3832.
41. Flaberg E, et al. (2011) High-throughput live-cell imaging reveals differential inhibition of tumor cell proliferation by human fibroblasts. *Int J Cancer* 128(12): 2793–2802.
42. Rathje L-SZ, et al. (2015) Oncogenes induce a vimentin filament collapse mediated by HDAC6 that is linked to cell stiffness. *Proc Natl Acad Sci USA* 111(4):1515–1520.
43. Nemeth JA, et al. (1999) Severe combined immunodeficient-hu model of human prostate cancer metastasis to human bone. *Cancer Res* 59(8):1987–1993.
44. Wang M, Stearns ME (1991) Isolation and characterization of PC-3 human prostatic tumor sublines which preferentially metastasize to select organs in S.C.I.D. mice. *Differentiation* 48(2):115–125.
45. Sugiyama N, et al. (2010) Fibroblast growth factor receptor 4 regulates tumor invasion by coupling fibroblast growth factor signaling to extracellular matrix degradation. *Cancer Res* 70(20):7851–7861.
46. Hutter JL, Bechhoefer J (1993) Calibration of atomic-force microscope tips. *Rev Sci Instrum* 64(7):1868–1873, and erratum (1993) 64(11):3342.
47. Chopinet L, Formosa C, Rols MP, Duval RE, Dague E (2013) Imaging living cells surface and quantifying its properties at high resolution using AFM in QI™ mode. *Micron* 48: 26–33.
48. Tseng Q, et al. (2011) A new micropatterning method of soft substrates reveals that different tumorigenic signals can promote or reduce cell contraction levels. *Lab Chip* 11(13):2231–2240.
49. Jeggari A, Alexeyenko A (2017) NEArender: An R package for functional interpretation of 'omics' data via network enrichment analysis. *BMC Bioinformatics*, in press.
50. Bayerlová M, et al. (2015) Comparative study on gene set and pathway topology-based enrichment methods. *BMC Bioinformatics* 16:334.
51. Alexeyenko A, Sonnhammer ELL (2009) Global networks of functional coupling in eukaryotes from comprehensive data integration. *Genome Res* 19(6): 1107–1116.